Saturable and reverse saturable absorption of Rhodamine B in methanol and water

N. K. M. Naga Srinivas, S. Venugopal Rao,* and D. Narayana Rao†

School of Physics, University of Hyderabad, Hyderabad 500 046, India

Received April 3, 2003; revised manuscript received July 23, 2003; accepted August 7, 2003

We have investigated nonlinear absorption of Rhodamine B dye in methanol and water near resonance (532 nm) on the higher-energy (435 nm) and lower-energy (600 nm) sides of the absorption band, using an open-aperture Z-scan technique with nanosecond pulses. We observed reverse saturable absorption (RSA) at 435 nm in both of the solvents, and a transition from saturable absorption (SA) to RSA with an increase in either intensity or concentration at 600 nm in methanol. A transition from RSA to SA with an increase in concentration at 600 nm was observed with water as the solvent. We used theoretical analysis based on rate equations to determine the two-photon and excited-state absorption coefficients from the experimental results.

OCIS codes: 190.0190, 190.4400, 160.4330, 140.2050.

1. INTRODUCTION

There is considerable interest in understanding the optical nonlinearities of dyes for widespread applications. Dye molecules are used mostly to generate tunable laser sources and in optical shutters, optical signal-processing devices,[1–4] two-photon microscopy,[5] upconversion lasers,[6,7] optical limiting,[8,9] optical data storage,[10,11] and three-dimensional microfabrication.[12] The investigation is ongoing for a new series of dyes, with large two-photon absorption (TPA) cross sections at shorter wavelengths which will have applications for the development of displays and blue–green lasers. The fluorescence yield and lasing efficiency of these organic dyes have been studied extensively. The basic absorption processes in dyes can be divided into linear and nonlinear absorption. Nonlinear absorption is a phenomenon defined as a nonlinear change (increase or decrease) in absorption with increasing intensity. This can be of either two types: saturable absorption (SA) and reverse saturable absorption (RSA). Depending on the pump intensity and on the absorption cross section at the excitation wavelength, most molecules show nonlinear absorption. With increasing intensity, if the excited states show saturation owing to their long lifetimes, the transmission will show SA characteristics. If, however, the excited state has strong absorption compared with that of the ground state, the transmission will show RSA characteristics. These absorption characteristics are highly dependent on the wavelength, intensity and excited-state lifetime. With the availability of intense laser sources it is essential to have perfect knowledge of the absorption characteristics of the medium. SA is vital for use of dyes in mode locking. The most important application of RSA is in an optical limiting device[13] that protects sensitive optical components, including the human eye, from laser-induced damage. RSA is observed as a result of excited-state absorption (ESA), TPA, or both. Among a variety of materials investigated for RSA, the best results were obtained for porphyrins,[14] phthalocyanines,[15] and fullerenes.[16] It is imperative to assess the nonlinear absorption at different wavelengths to determine the potential applications of these materials.

Rhodamine B dye belongs to the xanthene family. It is one of the most commonly used dyes in various spectroscopic studies. Our basic aim in the present study is to examine the nonlinear absorption behavior of Rhodamine B in the visible region, as most earlier studies were focused in the 690–1050 nm spectral region.[17,18] Our recent Z-scan and degenerate four-wave mixing studies with incoherent light suggested the presence of excited-state absorption (ESA) through resonant TPA in Rhodamine B.[19] There have been few reports on the nonlinear absorption properties suggesting the presence of TPA or ESA Rhodamine 6G.[20,21] Furthermore, a recent report suggests that a novel Rhodamine B cation fulleride salt shows strong optical limiting[22] at 532 nm and that the type of nonlinear absorption in Rhodamine B is saturable and the limiting action is due mainly to the fulleride salt. Here we report our results of nonlinear absorption in Rhodamine B at 435 and 600 nm in two solvents, for the first time to our knowledge, using the standard Z-scan technique.[23]

2. EXPERIMENT

A. Z Scan

The source for the experiments was a frequency-doubled Nd:YAG (Spectra-Physics INDI 40; 10 Hz, ~6 ns at 532 nm) laser, an anti-Stokes (435 nm) line from a 532 nm pumped Raman cell filled with hydrogen, and a dye laser (600 nm) that comprised an oscillator and a single-stage amplifier. Both the Raman cell and the dye laser were operated at 10 Hz and delivered pulses of nearly 6-ns duration. The laser medium, Rhodamine B in methanol, was transversely pumped by the second harmonic of Nd:YAG laser with a maximum output energy of ~100 mJ/pulse at 532 nm. The FWHM (spectral bandwidth) of the dye output was ~7 nm. Other essential details of the experimental setup can be found in Refs. 24–28. For the

open-aperture Z-scan experiments the input beam was focused with an 80-mm lens, and the sample was scanned across the focus with a micrometer translation stage controlled by a computer. The total transmitted light was collected with a large-area lens of $f \sim 120$ mm and focused onto a photodiode. Data acquisition was accomplished with a boxcar averager, an analog-to-digital converter card, and a PC. The beam waist at focus was estimated to be ~ 20 μm at 435 nm, ~ 27 μm at 532 nm, and ~ 35 μm at 600 nm. The corresponding peak intensities were estimated to be approximately, 10^8–10^9 W/cm^2. Neutral-density filters were used for controlling the intensity of input beam.

B. Measurements of Picosecond Fluorescence Lifetime

A mode-locked Tsunami picosecond laser second harmonic (375 nm; FWHM, ~ 1.2 ps) operated at 4 MHz was used as the excitation source. For decay measurements a fluorescence-lifetime spectrometer (IBH, UK, Model 5000U) was used. The excitation beam was focused in the sample, and fluorescence was collected at right angles to the excitation beam and detected by a microchannel plate–photomultiplier tube (Hamamatsu R3809U with a response time of ~ 0.15 ns) after passing through a monochromator. The signal from the photomultiplier tube was fed into the discriminator, and output from a discriminator served as a stop signal for a time-to-amplitude converter (TAC). The start signal was derived from a high-speed silicon detector (Thor Labs, Inc., DET210, with a response time of <1 ns). The photodiode signal was converted to transistor–transistor logic by a pulse converter (IBH, Model TB-01), and the output was used as start pulse for the TAC. The TAC output was fed to a multichannel analyzer card (Oxford Corporation, UK). Repetitive laser pulsing and collection of emitted photons produced a histogram of time versus counts that represented the fluorescence decay. The data analysis was carried out with the software provided by IBH (DAS-6), which was based on a reconvolution technique that used iterative nonlinear least-squares methods.

3. RESULTS AND DISCUSSION

Rhodamine B (>99% pure) dye solutions were prepared in 10^{-2}–10^{-5} M concentrations with highly purified spectroscopic grade methanol and Millipore water as the solvents. The linear absorption spectra for different concentrations were obtained with a UV–visible spectrometer, and the curves matched well those reported in literature. Representative absorption spectra of Rhodamine B in water (dashed curve) and methanol (solid curve) are shown in Fig. 1(a). Open-aperture Z scans were performed at different concentrations for various input intensities with 500 μm cuvettes at 435 and 600 nm excitation and with a 100 μm cuvette at 532 nm. The excitation wavelengths were chosen to probe the nonlinear absorption at off resonance (435 and 600 nm) and near resonance (532 nm) with the S_0–S_1 absorption band. The most general model for the organic molecule is a five-level system[29] [Fig. 1(b)] with S_0, S_1, S_n, T_1, and T_n states. Rate equations for this five-level model are

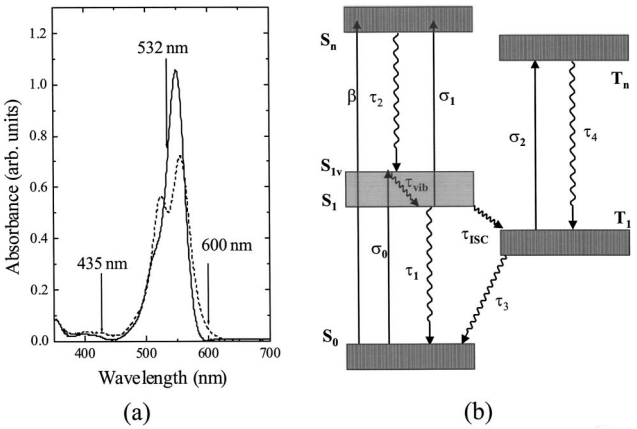

Fig. 1. (a) Absorption spectra of Rhodamine B in methanol (solid curve) and water (dashed curve). (b) Energy-level diagram of a typical Rhodamine B molecule: β, TPA coefficient; σ_0, ground-state absorption coefficient; σ_1, singlet-state absorption coefficient; σ_2, triplet-state absorption coefficient; τ_{S_1}, S_1-state lifetime; τ_{S_n}, S_n state lifetime; τ_{T_1}, T_1 state lifetime; τ_{T_n}, T_n state lifetime; τ_{vib}, vibrational relaxation time; τ_{ISC}, intersystem crossing time; S_0, S_1, S_n, singlet states; T_1, T_n, triplet states.

$$\frac{dN_0}{dt} = -\frac{\sigma_0 I N_0}{\hbar\omega} - \frac{\beta I^2}{2\hbar\omega} + \frac{N_1}{\tau_1} + \frac{N_3}{\tau_3}, \tag{1}$$

$$\frac{dN_1}{dt} = -\frac{\sigma_1 I N_1}{\hbar\omega} + \frac{\sigma_0 I N_0}{\hbar\omega} - \frac{N_1}{\tau_1} - \frac{N_1}{\tau_{\mathrm{ISC}}} + \frac{N_2}{\tau_2}, \tag{2}$$

$$\frac{dN_2}{dt} = \frac{\sigma_1 I N_1}{\hbar\omega} + \frac{\beta I^2}{2\hbar\omega} - \frac{N_2}{\tau_2}, \tag{3}$$

$$\frac{dN_3}{dt} = -\frac{\sigma_2 I N_3}{\hbar\omega} - \frac{N_3}{\tau_3} + \frac{N_1}{\tau_{\mathrm{ISC}}} + \frac{N_4}{\tau_4}, \tag{4}$$

$$\frac{dN_4}{dt} = \frac{\sigma_2 I N_3}{\hbar\omega} - \frac{N_4}{\tau_4}, \tag{5}$$

and the intensity transmitted through sample is

$$\frac{dI}{dz} = -\sigma_0 I N_0 - \sigma_1 I N_1 - \sigma_2 I N_3 - \beta I^2, \tag{6}$$

with

$$I = I_{00}\left[\frac{\omega_0^2}{\omega^2(z)}\right]\exp\left(\frac{-t^2}{\tau_p^2}\right)\exp\left[-\frac{2r^2}{\omega^2(z)}\right],$$

$$\omega(z) = \omega_0\left[1 + \left(\frac{z}{z_0}\right)^2\right]^{1/2}, \qquad z_0 = \frac{\pi\omega_0^2}{\lambda}, \tag{7}$$

where σ_0 is the ground-state absorption cross section, σ_1 and σ_2 are the excited-state absorption cross sections from states S_1 and T_1, respectively; β is the TPA coefficient; N_0, N_1, N_2, N_3, and N_4 represent the number densities of states S_0, S_1, S_n, T_1, and T_n, respectively; τ_{ISC} is the intersystem crossing time; τ_is are the lifetimes of the excited states; z_0 is the Rayleigh range; and ω_0 is the beam waist at focus. I is intensity as a function of radial parameter r, time t, and propagation direction z; I_{00} is the peak intensity at the focus of the Gaussian

beam, and τ_p is the input pulse width used. The differential equations were solved numerically by the Runge–Kutta fourth-order method. Equations were first decoupled and then integrated over time and length and along the radial direction. Assuming the input beam to be Gaussian, we varied the limits of integration for r, t, and z from 0 to ∞, $-\infty$ to ∞, and 0 to L (L is the length of the sample), respectively. Typical numbers of slices used for r, t, and z are 60, 30, and 5, respectively, and σ_1, σ_2, and β were then estimated through least-squares fit of the experimental data. We can clearly understand the various mechanisms that are responsible for the nonlinear behavior from the observed transmittance data and their five-level model analysis.

Depending on the input pulse's duration, nonlinear absorption in these materials normally occurs through transitions from $S_0 \rightarrow S_n$ states by instantaneous TPA or from $S_0 \rightarrow S_1 \rightarrow S_n$ states by a two-step resonant TPA (ESA if $S_1 \rightarrow S_n$ occurs after vibrational transitions or diffusion within the S_1) or $T_1 \rightarrow T_n$ states by means of ESA. For Rhodamine B the intersystem crossing time (τ_{ISC}), which is of the order of few microseconds, is of minor consequence because of the nanosecond and picosecond lifetimes of the singlet state. For the present studies we therefore can neglect intersystem crossing and hence the contribution of the T_1 state. Nonlinear absorption parameters were therefore calculated for an effective three-level system with S_0, S_1, and S_n states. We used the β value determined from the theoretical fits to calculate the TPA cross section (σ_{TPA}) from the following relation[30]:

$$\beta = \frac{N_0}{h\nu}\sigma_{\mathrm{TPA}}, \tag{8}$$

where h is Planck's constant, ν is the frequency of light, and N_0 is the number of molecules per unit volume.

Equations (9)–(11) below are used in the literature[31–33] for saturation of the first excited state. We incorporated these three equations into our five-level model to obtain best fits for the Z-scan curves. For the saturation of a homogeneously broadened line the dependence of measured absorption coefficient α on intensity I of the incident laser radiation is given by the expression[31]

$$\alpha = \alpha_0/1 + (I/I_s), \tag{9}$$

where α_0 is the low-intensity absorption coefficient and I_s is the saturation intensity.

A strong, narrow-band laser field saturates one segment of the inhomogeneous absorption profile (e.g., Doppler broadening), leading to decreased absorption. Malcuit *et al.*[32] proposed the following equation for this kind of inhomogeneous saturation:

$$\alpha = \frac{\alpha_0}{[1 + (I/I_s)]^{1/2}}. \tag{10}$$

Samoc *et al.*[33] observed SA in poly(indenofluorene), and they found that the experimental curves were not well reproduced by Eqs. (9) and (10), proposed the following *ad hoc* formula, and obtained a good fit:

$$\alpha = \frac{\alpha_0}{1 + (I/I_s)^{1/2}}. \tag{11}$$

A. Rhodamine B in Methanol

Off-resonance wavelength 435 nm was chosen as excitation wavelength, such that the excitation would be into the higher levels of the first excited state. Figure 2 shows open-aperture Z-scan curves at 435 nm at various concentrations for an intensity of 8.7×10^8 W/cm^2. Figure 2 also shows the theoretical curves (solid curves) generated with the three-level model. Figure 2(c) shows a solid curve with $\sigma_0 = 3.13 \times 10^{-19}$ cm^2, $\sigma_1 = 21.8 \times 10^{-18}$ cm^2, and $\beta = 30 \times 10^{-12}$ cm W^{-1}; scattered points ($\times$) generated with $\sigma_1 = 21.8 \times 10^{-18}$ cm^2 and $\beta = 0$; and a dotted curve generated with $\sigma_1 = 0$ and $\beta = 30 \times 10^{-12}$ cm W^{-1}. Figure 2(e) shows a solid curve with $\sigma_0 = 3.87 \times 10^{-19}$ cm^2, $\sigma_1 = 24.75 \times 10^{-18}$ cm^2, and $\beta = 40 \times 10^{-12}$ cm W^{-1}; scattered points ($\times$) generated with $\sigma_1 = 24.75 \times 10^{-18}$ cm^2 and $\beta = 0$; and a dotted curve generated with $\sigma_1 = 0$ and $\beta = 40 \times 10^{-12}$ cm W^{-1}. We can clearly see from Figs. 2(c) and 2(e) that the variation in σ_1 has a significant effect on the curve, implying that the curve does not show RSA behavior without ESA (σ_1). The effect of TPA (β) is negligible at this excitation. We obtain the best fits with lowest χ^2, however, by floating β and the σ_1 values, and these values are listed in Table 1. From the data we can see that with the increase in concentration the ESA cross section increases, thereby leading to an increase in

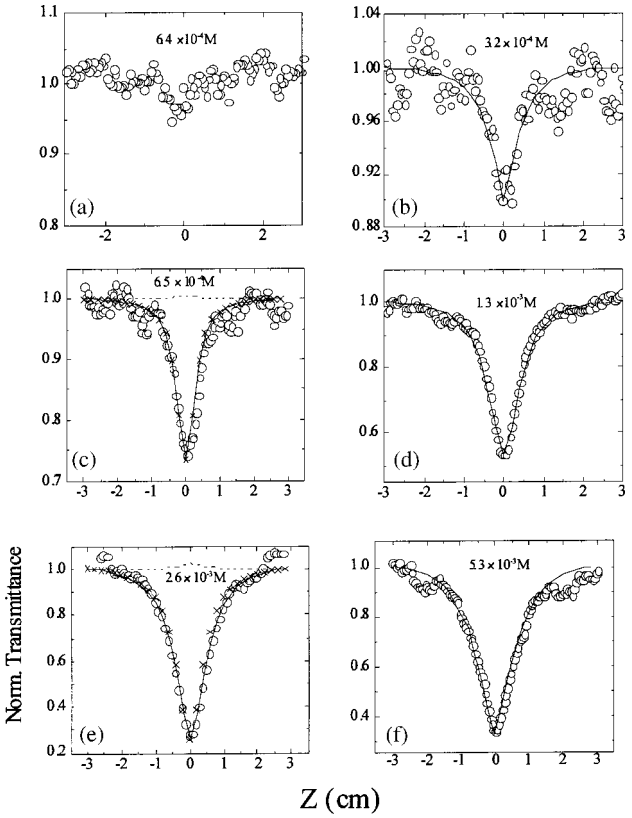

Fig. 2. Open-aperture Z-scan data of Rhodamine B in methanol at 435 nm at six concentrations at an intensity of ~9 $\times$ 10^8 W/cm^2.

Table 1. Excited-State Absorption Cross Sections σ and TPA Coefficient β at Several Concentrations of Rhodamine B in Methanol at 435 nm

Concentration (M)	σ_1 ($\times 10^{-18}$ cm^2)	β ($\times 10^{-12}$ cm W^{-1})	σ_{TPA} ($\times 10^{-50}$ cm^4 s)
5.3×10^{-3}	12.75	55	799.4
2.6×10^{-3}	24.75	40	1162
1.3×10^{-3}	21.8	20	1162
6.4×10^{-4}	21.8	30	3488
3.2×10^{-4}	8.0	20	4639

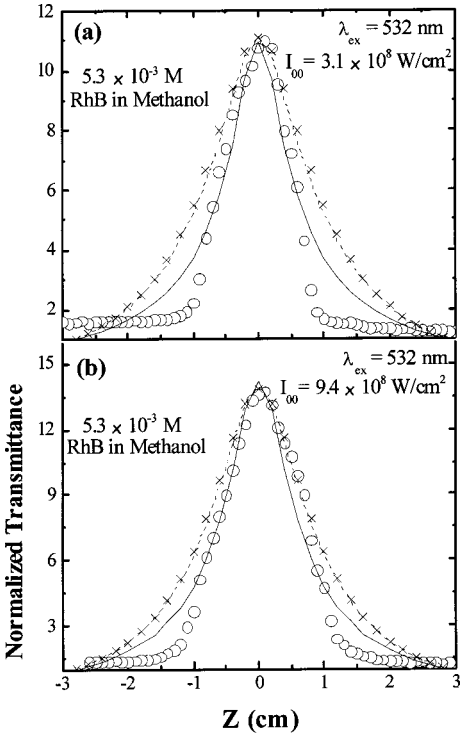

Fig. 3. Open-aperture Z-scan data of 5.3×10^{-3} M Rhodamine B in methanol.

nonlinear absorption. At low concentration the ESA cross section was 8×10^{-18} cm^2 and the linear transmittance was 80%; at high concentration the ESA cross section was 24.75×10^{-18} cm^2 and the linear transmittance was ~20%. At concentrations higher than 2.6×10^{-3} M we observe that the ESA coefficient falls down, which could be due mainly to the formation of aggregates. This result is in agreement with the observations made by Selwyn and Steidfeld.[34] This ESA behavior at 435 nm could be used for optical limiters because near this wavelength Rhodamine B exhibits minimum linear absorption.

To understand the behavior of the material near the absorption peak we obtained open aperture Z-scan curves at 532 nm. At this excitation wavelength, which is almost at the peak of the absorption band, an increase in transmission with increased intensity was observed (SA). In the vicinity of 532 nm the linear absorption coefficient is very large, and strong pumping leads to saturation rather than to RSA.[35] Open-aperture Z-scan curves at a concentration of 5.3×10^{-3} M at peak intensities of 3.1×10^8 and 9.39×10^8 W/cm^2 are depicted in Fig. 3. We observed dielectric breakdown for peak intensities above 1.4 GW/cm^2 as a result of heating caused by intense laser pulses, thereby reducing the transmitted intensity at focus. Equations (9)–(11) for the saturation of absorption were used to fit the Z-scan curves of Fig. 3. We found that Eq. (11) gives a better fit than the other two equations, and for the figure we derived all theoretical curves with $\sigma_1 = 2.0 \times 10^{-18}$ cm^2 and by varying saturation intensity I_s. In Fig. 3(a), scattered points (open circles) are the experimental data; crosses [×, Eq. (9)] represent the theoretical fit generated with $I_s = 0.13 \times 10^8$ W/cm^2; the dashed curve [Eq. (10)], the fit with $I_s = 0.68 \times 10^8$ W/cm^2; and the solid curve [Eq. (11)], the fit with $I_s = 1.8 \times 10^8$ W/cm^2. In Fig. 3(b) the scattered points (open circles) are the experimental data; the crosses [×, with Eq. (9)], the theoretical fit generated with $I_s = 0.48 \times 10^8$ W/cm^2; the dashed curve [Eq. (10)], the fit with $I_s = 0.26 \times 10^8$ W/cm^2; and the solid curve [Eq. (11)], the fit with $I_s = 9.3 \times 10^8$ W/cm^2. Sinha *et al.*[35] observed saturation behavior in Rhodamine B (ethanol) at 510 nm with 40-ns pulses, and they performed a closed-aperture Z-scan in order to investigate the thermal contribution. They observed the lowest thermal nonlinearity in an aqueous solution of the dye.

At 600 nm, the edge of the absorption band, we observed SA behavior for low intensities [Fig. 4(a) and Table 2]. For intensities below 4×10^8 W/cm^2, saturable absorption behavior was observed. At this wavelength the excitation is into the lowest of the S_1 energy levels, and therefore one expects more of localization of the energy,[36]

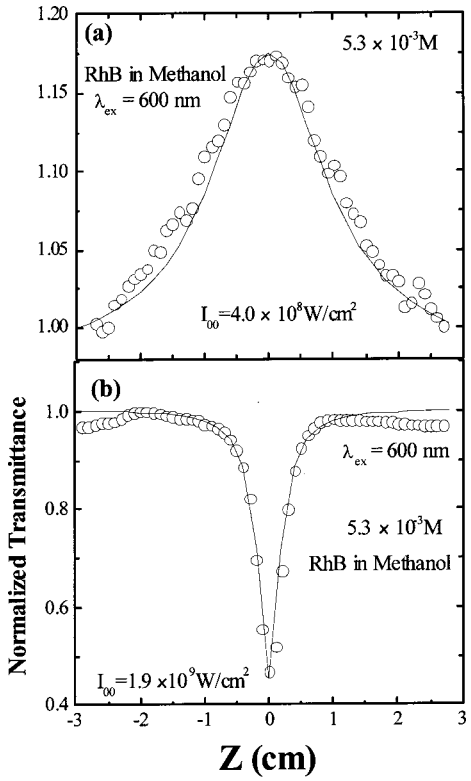

Fig. 4. Open-aperture Z-scan data of 5.3×10^{-3} M Rhodamine B in methanol at the intensities shown.

Table 2. Excited-State Cross Sections σ_1 TPA Coefficient β, and Singlet Lifetime τ at Three Concentrations of Rhodamine B in Methanol at 600 nm[a]

Concentration (M)	σ_1 ($\times 10^{-18}$ cm^2)	β ($\times 10^{-9}$ cm W^{-1})	σ_{TPA} ($\times 10^{-49}$ cm^4 s)	τ_{S_1} (ns)
1.0×10^{-2}	2.0	5.2	2739	3.79
5.3×10^{-3}	2.0	5.2	5479	3.79
2.6×10^{-3}	0.8	0		3.2

[a] For concentrations $<2.6 \times 10^{-3}$ M, no nonlinear absorption was observed.

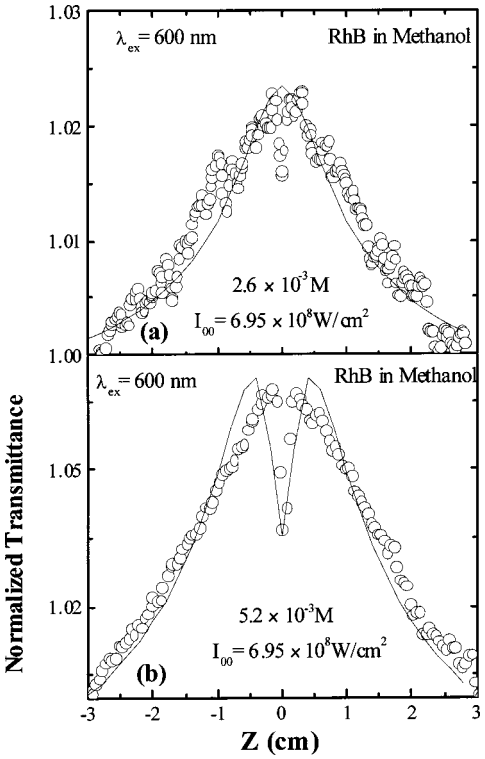

Fig. 5. Open-aperture Z-scan data of Rhodamine B in methanol.

thereby leading to saturation at lower intensities. As the intensity increased, the behavior switched to RSA, as shown in Fig. 4(b). The intensities used were 4.0×10^8 and 1.9×10^9 W/cm^2 for a concentration of 5×10^{-3} M. For increasing intensities ($>1.4 \times 10^9$ W/cm^2) the behavior shows a complete switchover from SA to RSA, which could probably be due to either TPA or ESA. At very large intensities ($\sim 1.9 \times 10^9$ W/cm^2) the behavior was completely dominated by RSA. Figure 4(a) shows the saturation curve for low intensity of 4×10^8 W/cm^2, and the theoretical curve was generated by incorporation of the saturation effect [with Eq. (11)] for level S_1 in an effective three-level model. In Fig. 4(a) the solid curve represents the curve with $\sigma_1 = 2.0 \times 10^{-18}$ cm^2 and $I_s = 0.2 \times 10^8$ W/cm^2. Figure 4(b) shows the RSA curve at the high intensity of 1.9×10^9 W/cm^2. The evaluated TPA coefficient at 600 nm was $\sim 0.58 \times 10^{-8}$ cm W^{-1}. We calculated the value of β for two extreme values of singlet-state excited-state absorption (σ_1). The observed change in transmission and shape of the curves was negligible for $\sigma_1 = 0$ and $\sigma_1 = 10 \times 10^{-19}$ cm^2, indicating that the predominant mechanism for nonlinear absorption in this case is TPA. This is in contrast to what we observed at 435 nm: a strong contribution from σ_1 with a small contribution from β to the RSA behavior. This result is expected, as the higher excited states of the singlet manifold relax to the lower vibrational states, leading to absorption of the pump laser from the lower singlet level to the higher excited states through ESA. When the excitation is directed to the lower side of the absorption band, as mentioned above, there is more localization of the energy before it decays to the ground state. This would, therefore, lead to resonant TPA.

The effect of concentration on transmission for a particular intensity ($\sim 7.0 \times 10^8$ W/cm^2) is shown in Fig. 5. Figure 5(a) shows the data for a 2.6×10^{-3} M concentration, and Fig. 5(b) shows the data for 5.3×10^{-3} M. As the concentration increased, we observed RSA within the SA. In Fig. 5(a) the solid curve was generated with $\sigma_1 = 2.05 \times 10^{-18}$ cm^2, $\beta = 0$ cm W^{-1}, and $I_s = 5.2 \times 10^8$ W/cm^2, and Fig. 5(b) shows a solid curve with $\sigma_1 = 2.05 \times 10^{-18}$ cm^2, $\beta = 52 \times 10^{-10}$ cm W^{-1}, and $I_s = 0.2 \times 10^8$ W/cm^2. Such behavior was reported earlier for zinc *meso*-tetra(*p*-methoxyphenyl) tetrabenzoporphyrin (ZnmpTBP),[37] polymethine dye,[38] and coordination compounds.[39] In ZnmpTBP the behavior was attributed to the excitation of population into higher excited states (T_n) at higher intensities, giving rise to RSA; and the SA behavior was given as due to the saturation of the T_1 state.[37] In polymethine dye[38] this behavior was attributed to irreversible damage induced by the input pulses. For ruthenium and osmium complexes of modified terpyridines,[39] the saturation curve was explained as being due to the compounds and the RSA portion as being due to TPA of the solvent and TPA, and the SA curves were superimposed to explain the observations. The most plausible explanation for the observed behavior in our case is that at higher concentrations these dye molecules tend to form aggregates. The presence of such aggregates can be easily identified through their linear absorption spectra, with new peaks appearing on S_0–S_1 absorption.[34] The appearance of new peaks in the absorption spectrum leads to the localization of excited energy in the S_1 states of different aggregates, thereby enhancing absorption from the S_1 to the S_n states, which follows the square law for intensity dependence, leading to enhanced TPA. At lower concentrations monomers are predominant and therefore excitation in the S_1 state diffuses owing to dephasing–vibrational relaxation within the S_1 state. The lifetimes of excited state S_1 for the various concentrations are obtained through fluorescence-lifetime measurements at room temperature. As the concentration was increased, we observed an increase in fluorescence lifetime from 2.6 to 3.8 ns, in agreement with the data available in literature.[40] These S_1 lifetimes were

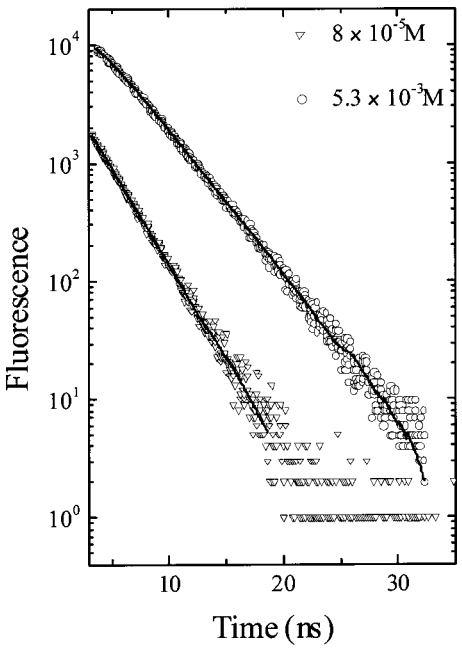

Fig. 6. Time-resolved fluorescence measurement of Rhodamine B in methanol at 8×10^{-5} and 5.3×10^{-3} M.

used for obtaining theoretical curves. Figure 6 shows the observed decay for two concentrations, 8×10^{-5} and 5×10^{-3} M.

B. Rhodamine B in Water

To evaluate the nonlinear absorption properties of Rhodamine B as a function of aggregates, we chose water as the solvent. In water the dye molecules aggregate at relatively lower concentrations. As in the case of methanol for off-resonance excitation of 435 nm, we observed RSA. As the excitation is into the higher energies of the first singlet state, this RSA is attributed to ESA rather than to TPA. The three-level model also revealed that the ESA contributes more than TPA at this excitation wavelength. These observations are similar to that for methanol as the solvent at 435 nm. Figure 7 shows open-aperture Z-scan curves and the corresponding theoretical curves at 435 nm at several concentrations at an intensity of 6.9×10^8 W/cm^2. Figure 7(c) shows a solid curve with $\sigma_1 = 17 \times 10^{-18}$ cm^2 and $\beta = 55 \times 10^{-12}$ cm W^{-1}; the crosses ($\times$) were generated with $\sigma_1 = 17 \times 10^{-18}$ cm^2 and $\beta = 0$, and the dashed curve was generated with $\sigma_1 = 0$ and $\beta = 55 \times 10^{-12}$ cm W^{-1}. Figure 7(e) shows a solid curve with $\sigma_1 = 26.5 \times 10^{-18}$ cm^2 and $\beta = 125 \times 10^{-12}$ cm W^{-1}; the dashed curve was generated with $\sigma_1 = 0$ and $\beta = 125 \times 10^{-12}$ cm W^{-1}; and the crosses ($\times$) were generated with $\sigma_1 = 26.5 \times 10^{-18}$ cm^2 and $\beta = 0$. σ_1 therefore shows a significant effect on the curve, whereas β does not have much influence on the shape of the curve. Therefore ESA (σ_1) contributes more to RSA behavior than does TPA at this excitation wavelength. The Z-scan curves for all the concentrations and their corresponding fits are shown in Fig. 7. The data obtained from the best fits for the various concentrations are listed in Table 3. At this excitation wavelength, Rhodamine B in the two solvents showed similar behavior, and the dominant mechanism was ESA rather than TPA. Observation of reduction in the ESA coefficient (σ_1) for the highest concentration of Rhodamine B in methanol is consistent with the steady decrease in the σ_1 value for increased concentration of Rhodamine B in water, as aggregation starts appearing even at low concentrations in water and one expects it at higher concentrations in methanol.

Z-scan curves obtained at 532 nm at two intensities, 1.8×10^8 and 1.4×10^8 W/cm^2, are very similar to those recorded with methanol as the solvent (Fig. 3). We generated theoretical curves by incorporating Eq. (11) into the three-level model with $\sigma_1 = 1.0 \times 10^{-19}$ cm^2 for both curves. Saturation intensities were $I_s = 0.16 \times 10^6$ and $I_s = 0.13 \times 10^6$ W/cm^2, respectively, for intensities 1.8×10^8 and 1.4×10^8 W/cm^2. After a particular threshold intensity we observed scattering from the material caused by dielectric breakdown. At intensities higher than this threshold, the Z-scan curves were not symmetric. For peak intensities above 1.8×10^8 W/cm^2 at high concentrations and 0.4×10^8 W/cm^2 at low concentrations we observed sudden decreases in the transmitted intensity.

The nonlinear absorption properties of Rhodamine B in water showed quite interesting behavior at 600 nm. For low intensities of nearly 3×10^8 W/cm^2 and at low concentrations, nonlinear absorption was not observed. For intensities near 6×10^8 W/cm^2, RSA was observed at low concentrations, and as the concentration increased a crossover from SA to RSA was observed. Excited state parameters σ_1, β, σ_{TPA}, and τ_{s1} calculated from the experimantal data for different concentrations are listed in

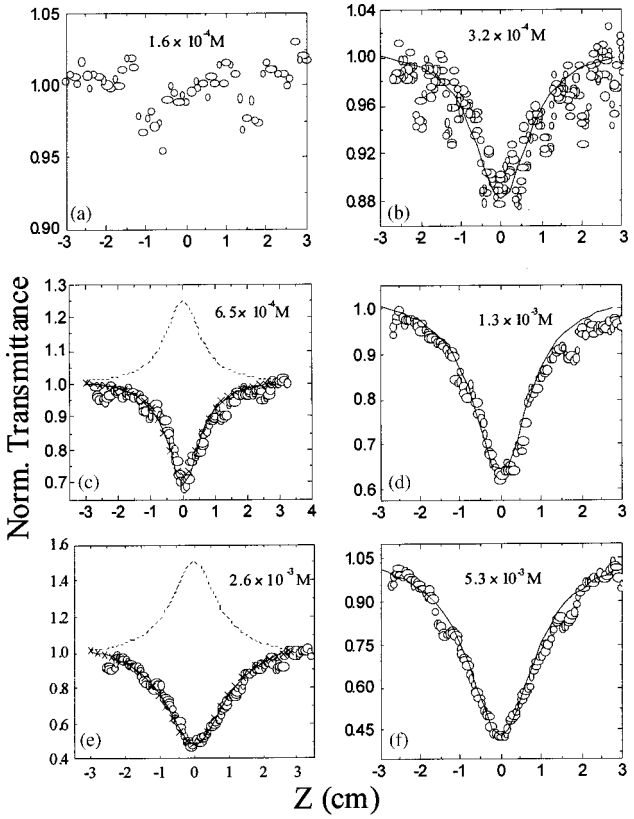

Fig. 7. Open-aperture Z-scan data of Rhodamine B in water at 435 nm at six concentrations at an intensity of 6×10^8 W/cm^2.

Table 3. Excited-State Absorption Cross Sections σ_1, TPA Coefficient β, and Singlet Lifetimes τ at Several Concentrations of Rhodamine B in Water at 435 nm at ~10^8 W/cm^2

Concentration (M)	σ_1 ($\times 10^{-18}$ cm^2)	β ($\times 10^{-12}$ cm W^{-1})	σ_{TPA} ($\times 10^{-49}$ cm^4 s)	τ_{S_1} (ns)
5.3×10^{-3}	10.8	55	80	1.04
2.6×10^{-3}	17	55	160	1.31
1.3×10^{-3}	18	55	320	1.41
6.4×10^{-4}	26.5	125	1453	1.41
3.2×10^{-4}	34.5	146	3375	1.43

Table 4. Excited-State Absorption Cross Sections σ_1 TPA coefficient β, and Singlet Lifetime τ at Several Concentrations of Rhodamine B in Water at 600 nm at ~6×10^8 W/cm^2

Concentration (M)	σ_1 ($\times 10^{-17}$ cm^2)	β ($\times 10^{-9}$ cm W^{-1})	σ_{TPA} ($\times 10^{-46}$ cm^4 s)	τ_{S_1} (ns)
1.0×10^{-2}	0.2	0		0.657
5.3×10^{-3}	0.2	0		1.04
2.6×10^{-3}	2	38	80.08	1.31
1.3×10^{-3}	2	50	210.75	1.41
6.4×10^{-4}	1.4	22	185.46	1.41
3.2×10^{-4}	1	21	354.06	1.43
1.6×10^{-4}	0.6	0.83	27.98	1.44

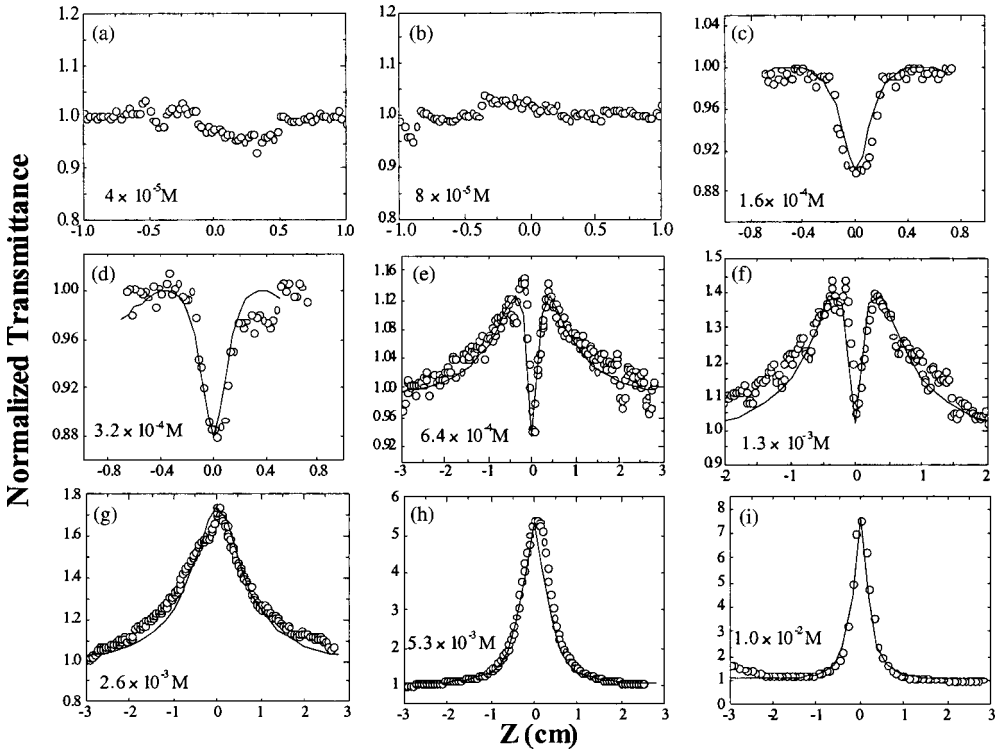

Fig. 8. Open-aperture Z-scan data Rhodamine B in water at nine concentrations at 600 nm at an intensity of 6×10^8 W/cm^2.

Table 4. The crossover from pure RSA to SA with RSA near $Z = 0$, and then to pure SA with a change in concentration at a peak intensity of ~6×10^8 W/cm^2, can be seen in Fig. 8. Figure 8(f) shows the data at a 1.3×10^{-3} M, concentration, the solid curve is a theoretical curve with $\sigma_1 = 2.0 \times 10^{-17}$ cm^2 and $\beta = 50 \times 10^{-9}$ cm W^{-1}. Figure 8(i) shows the data at a 1.0 $\times 10^{-2}$ M concentration; the solid curve is a theoretical curve generated with $\sigma_1 = 2.0 \times 10^{-18}$ cm^2. The RSA observed at lower concentration near focus is due predominantly to TPA. We observed a crossover from RSA to full SA behavior at a 2.6×10^{-3} M concentration at a

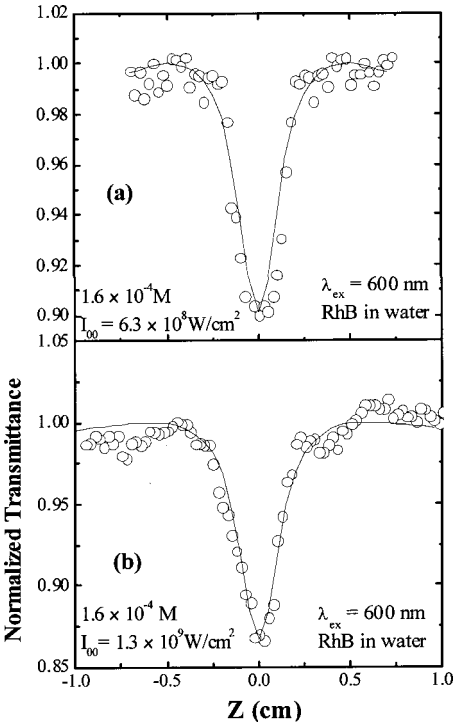

Fig. 9. Open-aperture Z-scan data of 1.6×10^{-4} M Rhodamine B in water at 600 nm.

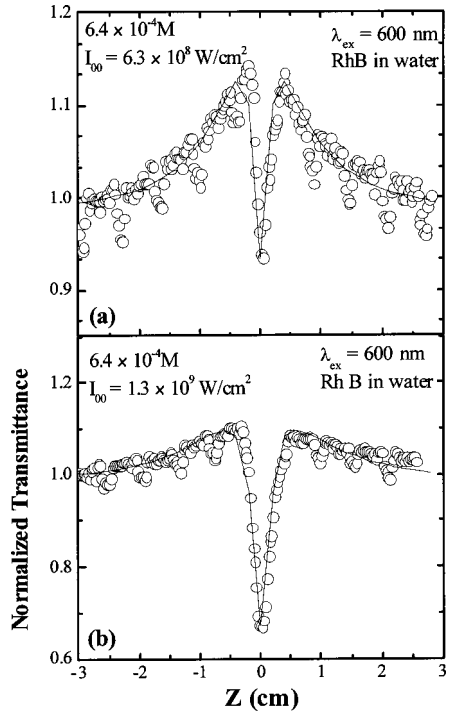

Fig. 10. Open-aperture Z-scan data of Rhodamine B in water at 6.3×10^{-4} M concentration.

peak intensity of $\sim 6 \times 10^8$ W/cm^2. We did not observe any nonlinear absorption for 10^{-5} M concentration.

To study complex absorption behavior we used three concentrations, each of which showed a different behavior. Figure 9 shows the open-aperture Z-scan curves for a concentration of 1.6×10^{-4} M at two intensities, 6.3×10^8 and 1.3×10^9 W/cm^2. Figure 9(a) shows a theoretical fit with $\sigma_1 = 6 \times 10^{-17}$ cm^2 and $\beta = 8.55 \times 10^{-9}$ cm W^{-1} at $I_{00} = 1.3 \times 10^9$ W/cm^2. In Fig. 9(b) a theoretical curve generated with $\sigma_1 = 0$ cm^2 and $\beta = 0.83 \times 10^{-9}$ cm W^{-1} is represented by the solid curve. For similar concentrations we observed linear absorption in methanol for a pump intensity of 6.5×10^8 W/cm^2. Figure 10 shows nonlinear absorption behavior at a 6×10^{-4} M concentration for two intensities. An intensity-dependent study at a 6.4×10^{-4} M concentration revealed that the RSA observed near focus was TPA dominant. The solid curve in Fig. 10(a) was generated with $\sigma_1 = 14 \times 10^{-18}$ cm^2 and $\beta = 22 \times 10^{-9}$ cm W^{-1} for the experimental data obtained with 6.3×10^8 W/cm^2. In Fig. 10(b) the scattered points (open circles) show the open-aperture data at 1.3×10^9 W/cm^2 and the solid curve is a theoretical fit generated with $\sigma_1 = 14 \times 10^{-18}$ cm^2 and $\beta = 28 \times 10^{-9}$ cm W^{-1}. The highly concentrated (1×10^{-2} M) solution shows saturation behavior at low and high intensities.

Earlier studies revealed that Rhodamine B has zwitterionic form in water[41] and forms aggregates at lower concentrations than do other organic solvents. Smirl *et al.*[42] observed an increase in dimer-to-monomer ratio with an increase in concentration. They observed a variation in the dimer-to-monomer ratio from 0.06 to 1.61 with concentrations ranging from 10^{-5} to 10^{-3} M. They also observed rapid fluorescence decay at high concentrations, and their measurements suggested that energy transfer can be a primary pathway for the decay of the excited-state monomer.

Smith *et al.*[43] observed a transition from RSA to SA with increasing gold nanoparticle content in hexamethyindotricarboncyanine iodide in a methanol–water mixture. They attributed this transition to the sign reversal of $\chi^{(3)}$ caused by the modification of the local field factor

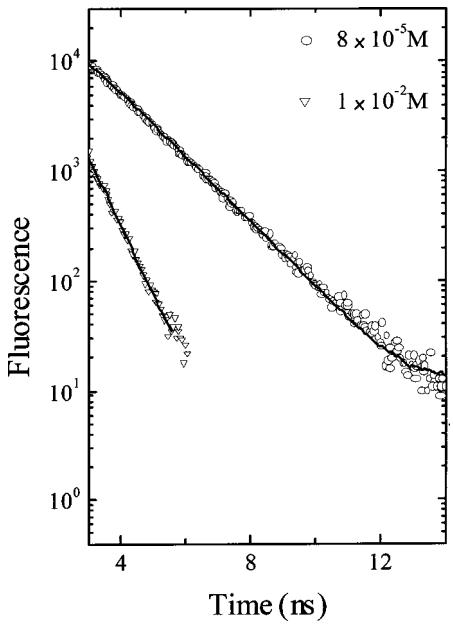

Fig. 11. Time-resolved fluorescence measurement of Rhodamine B in water at 8×10^{-5} and 1.0×10^{-2} M.

at the surface plasmon resonance. Zhan *et al.*[44] observed a similar transition in a charge-transfer salt [$(TBA)_2$ Ni$(dmit)_2$, where TBA is tetra-*n*-butylammonium, and dmit is 2-thioxo-1,3-dithiole-4,5-dithiolate] with increasing intensity. They attributed this transition to fifth-order nonlinearity, as the excitation wavelength was 1064 nm and absorption peaked near 532 nm for their sample.

Aggregation of molecules in water is expected to increase the localization of energies and thereby lead to enhancement of TPA. Although we saw a slight improvement of the TPA coefficient in water compared with the methanol solution, it was not proportional to the amount of increase in the aggregation as seen from the absorption spectrum. To understand this, we performed lifetime measurements of the first excited state in water and methanol. We observed that the fluorescence lifetimes were much smaller in water than in methanol. We observed no variation in fluorescence decay until a concentration of 1.3×10^{-3} M was reached and observed a sudden fall from ~1.4 ns to 657 ps at a 1×10^{-2} M concentration. These results are in agreement with previously reported values.[42] Fluorescence decay times at two concentrations are shown in Fig. 11. The solid curves through the data are fits of single exponentials. This fast decay has been attributed to energy transfer from the monomer to the nonradiatively decaying dimer.[42] Aggregation is known to lead to the reduction in lifetimes of S_1 state emission from singlets owing to fast energy transfer from monomers to dimers through self-absorption of the radiation and nonradiative emission from the dimers. A longer lifetime and more localization of the energy would have increased the RSA behavior. Theoretical fits of the experimental data, too, yielded consistent results with the available data on the lifetimes of the excited states. Lifetimes calculated from the observed data for water and methanol as solvents are τ_{s1}(methanol) = 2.6 ns and τ_{s1}(water) = 1.4 ns. These values agree reasonably well with the values from picosecond lifetime measurements.

From these observations we conclude that the RSA behavior at low concentrations with 600-nm excitation is due mainly to resonant TPA from the monomers. As the concentration increased, the absorption cross section also increased at 600 nm. Longer lifetimes of the monomers led to saturation behavior. For higher concentrations we observed pure SA behavior caused by rapid energy distribution among the monomers and dimers. The reduction in the width of the SA curve can be attributed to fast decay of the dimers (<200 ps), which are populated through energy transfer from the monomers excited at 600 nm. Such fast decay requires large intensities for saturating the levels.

4. CONCLUSIONS

In summary, our Z-scan experiments have revealed interesting features of the nonlinear absorption properties of Rhodamine B in methanol and in water. At 435 nm excitation RSA was observed in both of those solvents, predominantly because of excited-state absorption. With increasing concentration the nonlinear absorption increased in both cases. At resonance (532 nm), SA was observed in both solvents, as the excitation was directed into the first excited state. At 600 nm excitation a switchover from SA to RSA behavior was observed with increasing intensity or with increasing concentration in methanol and vice versa in water. We attribute the behavior in methanol to the localization of energy, which leads to resonant TPA. In water the changeover from RSA to SA is attributed to the aggregation and fast decay times of dimers, which get populated through energy transfer.

ACKNOWLEDGMENTS

D. N. Rao acknowledges the support of the Department of Atomic Energy–Board of Research in Nuclear Science and the Defense Research and Development Organization, India. We thank the National Center for Ultrafast Processes (Chennai, India) for extending to us the use of their picosecond fluorescence lifetime measurements facility.

*Present address: Centre for Ion Beam Applications, Department of Physics, Faculty of Science, Block S12, 2 Science Drive 3, National University of Singapore, Singapore 117542. E-mail: physvr@nus.edu.sg.

†Address for correspondence: dnrsp@uohyd.ernet.in.

REFERENCES

1. F. P. Schafer, *Dye Lasers* (Springer-Verlag, Berlin, 1973).
2. R. L. Sutherland, *Handbook of Nonlinear Optics* (Marcel Dekker, New York, 1996).
3. H. S. Nalwa and S. Miyata, *Nonlinear Optics of Organic Molecules and Polymers* (CRC Press, Boca Raton, Fla., 1997).
4. F. P. Schafer, "Organic dyes in laser technology," Angew. Chem. Int. Ed. Eng. **9**, 9–25 (1970).
5. W. Denk, J. H. Strickler, and W. W. Webb, "Two-photon laser scanning fluorescence microscopy," Science **24**, 73–76 (1990).
6. M. Anandi, "Two-photon pumped unconverted lasing in dye doped polymer waveguides," Appl. Phys. Lett. **62**, 3423–3425 (1993).
7. G. S. He, C. F. Zhao, J. D. Bhawalkar, and P. N. Prasad, "Two-photon pumped cavity lasing in novel dye doped bulk matrix rods," Appl. Phys. Lett. **67**, 3703–3705 (1995).
8. J. E. Ehrilich, X. L. Wu, I. Y. S. Lee, Z. Y. Hu, H. Rockel, S. R. Marder, and J. W. Perry, "Two-photon absorption and broadband optical limiting with bis-donor stilbenes," Opt. Lett. **22**, 1843–1845 (1997).
9. G. S. He, G. Xu, P. N. Prasad, B. A. Reinhardt, J. C. Bhatt, and A. G. Dillard, "Two-photon absorption of novel organic compounds," Opt. Lett. **20**, 435–437 (1995).
10. D. A. Parthenopoulos and P. M. Rentzepis, "Three-dimensional optical storage memory," Science **245**, 843–845 (1989).
11. H. Strickler and W. W. Webb, "Three-dimensional optical data storage in refractive media by two-photon excitation," Opt. Lett. **16**, 1780–1782 (1991).
12. B. H. Cumpston, S. P. Ananthavel, S. Barlow, D. L. Dyer, J. E. Ehrlich, L. L. Erskine, A. A. Heikal, S. M. Kuebler, I. Y. S. Lee, D. M. Maughon, J. Quin, H. Rockel, M. Rumi, and J. W. Perry, "Two-photon polymerization initiators for three-dimensional optical data storage and microfabrication," Science **398**, 51–54 (1999).
13. L. W. Tutt and T. F. Boggess, "A review of optical limiting mechanisms and devices using organics, fullerenes, semiconductors and other materials," Prog. Quantum Electron. **17**, 299–338 (1993).

14. A. Krivokapic, H. L. Anderson, G. Bourhill, R. Ives, S. Clark, and K. J. McEwan, "Meso-tetra-alkynyl porphyrins for optical limiting—A survey of Group III and IV metal complexes," Adv. Mater. **13**, 652–656 (2001).
15. M. Hanack, T. Schneider, M. Barthel, J. S. Shirk, S. R. Flom, and R. G. S. Pong, "Indium phthalocyanines and naphthalocyanines for optical limiting," Coord. Chem. Rev. **219**, 235–258 (2001).
16. L. W. Tutt and A. Kost, "Optical limiting performance of C_{60} and C_{70} solutions," Nature **356**, 225–226 (1992).
17. C. Xu and W. W. Webb, "Measurement of two-photon excitation cross sections of molecular fluorophores with data from 690 to 1050 nm," J. Opt. Soc. Am. B **13**, 481–491 (1996).
18. A. Fischer, C. Cremer, and E. H. K. Stelzer, "Fluorescence of coumarins and xanthenes after two-photon absorption with a pulsed titanium-sapphire laser," Appl. Opt. **34**, 1989–2003 (1995).
19. S. V. Rao, N. K. M. N. Srinivas, and D. N. Rao, "Nonlinear absorption and excited state dynamics in Rhodamine B studied using Z-scan and degenerate four wave mixing techniques," Chem. Phys. Lett. **361**, 439–445 (2002).
20. C. V. Bindhu, S. S. Harilal, V. P. N. Nampoori, and C. P. G. Vallabhan, "Studies of nonlinear absorption and aggregation in aqueous solutions of Rhodamine 6G using a transient thermal lens technique," J. Phys. D **32**, 407–411 (1999).
21. P. Sathy, R. Philip, V. P. N. Nampoori, and C. P. G. Vallabhan, "Photoacoustic observation of excited state absorption in the laser dye Rhodamine 6G," J. Phys. D **27**, 2019–2022 (1994).
22. C. Liu, Q. Gong, Y. Chen, H. Chen, and D. Qiang, "Reverse saturable absorption of a novel Rhodamine B cation fulleride salt at 532 nm," Appl. Phys. A **73**, 477–479 (2001).
23. M. Sheik-Bahae, A. A. Said, T.-H. Wei, D. J. Hagan, and E. W. Van Stryland, "Sensitive measurement of optical nonlinearities using a single beam," IEEE J. Quantum Electron. **26**, 760–769 (1990).
24. D. N. Rao, S. V. Rao, F. J. Aranda, M. Nakashima, and J. A. Akkara, "Ultrafast relaxation times of metalloporphyrins by time-resolved degenerate four-wave mixing with incoherent light," J. Opt. Soc. Am. B **14**, 2710–2715 (1997).
25. S. V. Rao, L. Giribabu, B. G. Maiya, and D. N. Rao, "A novel observation in the measurement of ultrafast relaxation times using incoherent light," Curr. Sci. **72**, 957–960 (1997).
26. S. V. Rao and D. N. Rao, "Excited state dynamics of C_{60} studied using incoherent light," Chem. Phys. Lett. **283**, 227–230 (1997).
27. S. V. Rao, N. K. M. N. Srinivas, L. Giribabu, B. G. Maiya, D. N. Rao, R. Philip, and G. R. Kumar, "Excited state dynamics in tetratolyl porphyrins studied using degenerate four wave mixing with incoherent light and ps pulses," Opt. Commun. **192**, 123–133 (2001).
28. S. V. Rao and D. N. Rao, "Excited state dynamics of phthalocyanines studied using degenerate four wave mixing with incoherent light," J. Porphyr. Phthalocyan. **6**, 233–238 (2002).
29. S. V. Rao, D. N. Rao, J. A. Akkara, B. S. DeCristofano, and D. V. G. L. N. Rao, "Dispersion study of nonlinear absorption in C_{60} using Z-scan," Chem. Phys. Lett. **297**, 491–498 (1998).
30. G. S. He, J. D. Bhawalkar, C. F. Zhao, and P. N. Prasad, "Optical limiting effect in a two-photon absorption dye doped solid matrix," Appl. Phys. Lett. **67**, 2433–2435 (1995).
31. A. E. Siegman, *Lasers* (University Science, Mill Valley, Calif., 1986), p. 207.
32. M. S. Malcuit, R. W. Boyd, L. W. Hillman, J. Krasinski, and C. R. Stroud, Jr., "Saturation and inverse-saturation absorption line shapes in alexandrite," J. Opt. Soc. Am. B **1**, 73–75 (1984).
33. M. Samoc, A. Samoc, B. L. Davies, H. Reish, and U. Scherf, "Saturable absorption in poly(indenofluorene): a picket-fence polymer," Opt. Lett. **23**, 1295–1297 (1998).
34. J. E. Selwyn and J. I. Steidfeld, "Aggregation equilibria of xanthene dyes," J. Phys. Chem. **76**, 762–774 (1972).
35. S. Sinha, A. Ray, and K. Dasgupta, "Solvent dependent nonlinear refraction in organic dye solution," J. Appl. Phys. **87**, 3222–3226 (2000).
36. G. B. Talapatra, D. N. Rao, and P. N. Prasad, "Spectral diffusion within the inhomogeneously broadened n-π^* singlet–triplet transition of the orientationally disordered solid of 4-bromo-4′-chlorobenzophenone," J. Phys. Chem. **88**, 4636–4640 (1984).
37. N. K. M. N. Srinivas, S. V. Rao, D. V. G. L. N. Rao, B. K. Kimball, M. Nakashima, B. S. Decristofano, and D. N. Rao, "Wavelength dependent studies of nonlinear absorption in zinc *meso*-tetra(*p*-methoxyphenyl)tetrabenzoporphyrin (Znmp TBP) using Z-scan technique," J. Porphyri. Phthalocyn. **5**, 549–554 (2001).
38. O. V. Przhonska, J. H. Lim, D. J. Hagan, E. W. Van Stryland, M. V. Bondar, and Y. L. Slominsky, "Nonlinear light absorption of polymethine dyes in liquid and solid media," J. Opt. Soc. Am. B **15**, 802–809 (1998).
39. M. Konstantaki, E. Koudoumas, S. Couris, P. Laine, E. Amouyal, and S. Leach, "Substantial non-linear optical response of new polyads based on Ru and Os complexes of modified terpyridines," J. Phys. Chem. B **105**, 10,797–10,804 (2001).
40. P. C. Beaumont, D. G. Johnson, and B. J. Parsons, "Photophysical properties of laser dyes: picosecond laser flash photolysis studies of Rhodamine 6G, Rhodamine B and Rhodamine 101," J. Chem. Soc. Faraday Trans. **89**, 4185–4191 (1993).
41. I. L. Arbeloa and K. K. Rohatgi-Mukherjee, "Solvent effect on photophysics of the molecular forms of Rhodamine B. Solvation models and spectroscopic parameters," Chem. Phys. Lett. **128**, 474–479 (1986).
42. A. L. Smirl, J. B. Clark, E. W. Van Stryland, and B. R. Russell, "Population and rotational kinetics of the Rhodamine B monomer and dimer: picosecond transient spectrometry," J. Chem. Phys. **77**, 631–640 (1982), and references therein.
43. D. D. Smith, G. Fischer, R. W. Boyd, and D. A. Gregory, "Cancellation of photoinduced absorption in metal nanoparticle composites through a counterintuitive consequence of local field effects," J. Opt. Soc. Am. B **14**, 1625–1631 (1997).
44. C. Zhan, W. Xu, D. Zhang, D. Li, Z. Lu, Y. Nie, and D. Zhu, "Z-scan investigation of fifth-order optical nonlinearity induced by saturable-absorption from $(TBA)_2Ni(dmit)_2$: application for optical limiting," J. Mater. Chem. **12**, 2945–2948 (2002).